

## Fast 3D target-oriented reverse-time datuming

Shuqian Dong<sup>1</sup>, Yi Luo<sup>2</sup>, Xiang Xiao<sup>3</sup>, Sergio Chávez-Pérez<sup>4</sup>, and Gerard T. Schuster<sup>5</sup>

### ABSTRACT

Imaging of subsalt sediments is a challenge for traditional migration methods such as Kirchhoff and one-way wave-equation migration. Consequently, the more accurate two-way method of reverse-time migration (RTM) is preferred for subsalt imaging, but its use can be limited by high computation cost. To overcome this problem, a 3D target-oriented reverse-time datuming (RTD) method is presented, which can generate redatumed data economically in target areas beneath complex structures such as salt domes. The redatumed data in the target area then can be migrated inexpensively using a traditional migration method. If the target area is much smaller than the acquisition area, computation costs are reduced significantly by the use of a novel bottom-up strategy to calculate the extrapolated Green's functions. Target-oriented RTD is tested on 2D and 3D SEG/EAGE synthetic data sets and a 3D field data set from the Gulf of Mexico. Results show that target-oriented RTD combined with standard migration can image sediments beneath complex structures accurately with much less calculation effort than full volume RTM. The requirement is that the area over the target zone is smaller than that of the acquisition survey.

### INTRODUCTION

Kirchhoff migration is considered the most commonly used 3D prestack migration algorithm because of its speed and stability advantages, but it has difficulty imaging complex structures. This is because standard Kirchhoff migration is based on a high-frequency ray approximation, which typically accounts for single arrivals but ignores multipathing effects. One-way wave-equation-based depth

migration can be used to handle multipathing events (Claerbout, 1971, 1985), but this method has a dip limitation and problems in handling multiples and turning waves. Accounting for defocusing effects, multiple arrivals, and turning waves caused by complex velocity distributions is one of the biggest challenges in exploration seismology (Gray et al., 2001).

Generally, it is agreed that full-wave-equation (two-way wave) migration is more accurate for imaging reflections that propagate through structures in highly complex media (Biondi et al., 2002) if an accurate migration velocity is used. One example is reverse-time migration (RTM). Based on the full solution of the two-way wave equation, RTM is not dip-limited compared to one-way imaging methods and accounts for wave propagation in any direction (Baysal et al., 1983; McMechan, 1983; Whitmore, 1983; Esmersoy and Oristaglio, 1988). Moreover, RTM accounts for multiples and turning waves. Therefore, it computes more accurate seismic images than Kirchhoff migration in highly complex media. However, RTM is not used often in industry because it is computationally expensive for 3D prestack migration. The high computation cost arises from solving the two-way wave equation and the high storage cost for a 3D implementation. Symes (2007) introduces an optimal checkpointing technique to avoid the significant storage requirement for 3D RTM, but the tradeoff is additional computation time.

Several methods have been proposed recently to overcome the high computation and memory storage requirements of RTM. Schuster (2002) shows that RTM is equivalent to a generalized diffraction-stack migration. Zhou and Schuster (2002) develop a wavefront RTM technique where the wave propagation equation is solved only in the wavefront zone to reduce computation costs. Cao (2007) implements the 3D case for this method. Based on the idea of generalized diffraction stack migration, Luo (internal report, 2002) and Luo and Schuster (2004) propose a target-oriented reverse-time datuming (RTD) method, where computation costs can be reduced significantly for target-oriented imaging. As a validation, Zhou and Luo

Manuscript received by the Editor 23 December 2008; revised manuscript received 28 May 2009; published online 15 December 2009.

<sup>1</sup>Formerly University of Utah, Department of Geology and Geophysics, Salt Lake City, Utah, U.S.A.; presently TGS-NOPEC Geophysical Company, Houston, Texas, U.S.A. E-mail: shdong@gmail.com.

<sup>2</sup>Saudi Aramco, Dhahran, Saudi Arabia; E-mail: yi.luo@aramco.com.

<sup>3</sup>Formerly University of Utah, Department of Geology and Geophysics, Salt Lake City, Utah, U.S.A.; presently Nexus Geoscience, Inc., Sugarland, Texas, U.S.A. E-mail: xiangxiaoutah@gmail.com.

<sup>4</sup>Instituto Mexicano del Petróleo, Mexico City, Mexico. E-mail: schavez@imp.mx.

<sup>5</sup>University of Utah, Department of Geology and Geophysics, Salt Lake City, Utah, U.S.A. E-mail: j.schuster@utah.edu.

© 2009 Society of Exploration Geophysicists. All rights reserved.

(internal report, 2002) present 2D examples, followed by Dong et al. (2007) who present 3D examples of target-oriented RTD. Based on the target-oriented RTD method, Liu and Wang (2008) omit the redatuming step and apply the imaging condition directly to the target areas. In a related effort, Wang et al. (2006) combine one-way wave-equation-based redatuming and Kirchhoff-based migration to improve the speed and quality of subsalt velocity analysis.

In this work, we present the theory and application of the 3D target-oriented RTD method. As a computationally inexpensive alternative to RTM, reverse-time datuming extrapolates the wavefield to a subsalt artificial datum using the expensive but accurate finite-difference (FD) solutions to the full wave equation. In the redatuming step, only the velocity model above the datum is needed for the FD solutions. Furthermore, a bottom-up strategy can reduce FD computation by more than an order of magnitude for typical target-oriented applications. After redatuming, a less expensive method such as phase shift or Kirchhoff migration can be used because the sediments below the datum usually have less complex structures.

First, we present the theory of target-oriented RTD, then show several numerical results. We test the target-oriented RTD method on 2D and 3D SEG/EAGE synthetic data and demonstrate an application of this method on a 3D field data set from the Gulf of Mexico. For all these tests, Kirchhoff migration is applied to the original and redatumed data.

## THEORY

Luo (internal report, 2002) and Luo and Schuster (2004) propose target-oriented RTD as a cheap and efficient alternative to full-volume RTM. Reverse-time datuming can be understood as backpropagating wavefields from both the source and receiver sides (Berryhill, 1979, 1984, 1986; Yilmaz and Lucas, 1986; Bevc, 1995) or as a correlation transform from surface seismic profile (SSP) data to single-well profile (SWP) data (Schuster, 2009), as demonstrated in Figure 1. The transform is described mathematically by the acoustic reciprocity equation of correlation type (Wapenaar, 2004; Schuster, 2009), given as

$$\begin{aligned} \mathbf{A}, \mathbf{B} \in S_{\text{datum}}; \quad & \overbrace{\text{Im}[G(\mathbf{A}|\mathbf{B})]}^{\text{SWP}} \\ \approx 2ik^2 \int_{S_0} \int_{S'_0} & \overbrace{G(\mathbf{A}|\mathbf{y})}^{\text{VSP}} * \overbrace{G(\mathbf{y}|\mathbf{x})}^{\text{SSP}} \overbrace{G(\mathbf{B}|\mathbf{x})}^{\text{VSP}} * d^2y d^2x, \end{aligned} \quad (1)$$

where  $\mathbf{x}$  and  $\mathbf{y}$  are the locations of sources and receivers near the surface, and  $\mathbf{A}$  and  $\mathbf{B}$  are along the datum line. The Green's function  $G$

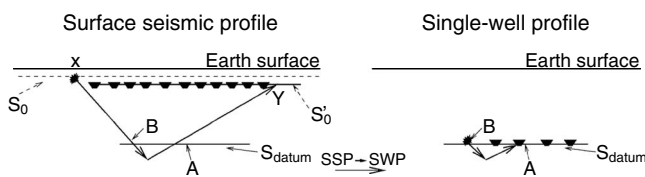


Figure 1. Diagram demonstration for SSP  $\rightarrow$  SWP correlation transform. The left panel depicts a SSP survey, where receivers are along  $S_0$  and sources are distributed along line  $S_0$ . Right panel depicts a redatumed SWP survey, where the virtual sources and receivers are distributed at datum line  $S_{\text{datum}}$ .

$G(\mathbf{A}|\mathbf{B})$  represents the harmonic point-source response of the media, where the source is located at  $\mathbf{B}$  and the receiver is located at  $\mathbf{A}$ . Here,  $G(\mathbf{A}|\mathbf{y})$  and  $G(\mathbf{B}|\mathbf{x})$  are the VSP Green's functions for harmonic point sources in an acoustic medium with variable velocity and constant density, and  $G(\mathbf{y}|\mathbf{x})$  is the SSP Green's function where both the source and receiver are near the surface. The derivation of this equation is given in Appendix A.

Luo and Schuster (2004) suggested that, in a target-oriented mode, an efficient way to calculate the vertical seismic profile (VSP) Green's functions is to locate the sources at the datum and the receivers at the near surface. As an example, Figure 2a shows that, e.g., 13 FD solutions (for the 13 sources along  $S_0$ ) are needed to compute the extrapolator kernel  $G(\mathbf{A}|\mathbf{y})$  and Figure 2b suggests that only five FD solutions (for the five sources along  $S'_0$ ) are needed to find  $G(\mathbf{y}|\mathbf{A})$ . In this example, area  $S'_0$  on the subsurface is assumed to be smaller than the area covered by the sources along  $S_0$ . Thus, it is cheaper computationally to use an FD solver first to compute  $G(\mathbf{y}|\mathbf{A})$  (for sources along the small horizontal buried plane  $S'_0$ ) and then use the reciprocity relationship to find the Green's functions for sources along the surface, i.e.,  $G(\mathbf{A}|\mathbf{y}) = G(\mathbf{y}|\mathbf{A})$ .

Table 1 shows examples of the CPU costs of standard datuming and the target-oriented approach. The bottom-up method does not save computation time if the area of the target subsurface is the same as that of the top surface in the 2D SEG/EAGE salt example. However, the bottom-up approach can save up to 90% of computation costs if the target subsurface is smaller than the top surface. These savings can be even higher if the target subsurface is less than several times smaller than the acquisition area on the surface.

## RTD algorithm

Figure 3 shows the five-step workflow of the target-oriented RTD method:

- 1) Calculate the VSP Green's functions  $G(\mathbf{x}|\mathbf{A})$  by finite-difference methods, where  $\mathbf{x}$  is at the near surface and  $\mathbf{A}$  is at the new datum. In this case, the FD solutions are a set of band-limited Green's functions with the same bandwidth as the data.
- 2) Use reciprocity to get the Green's functions  $G(\mathbf{A}|\mathbf{x})$ .
- 3) Transform the SSP seismic data  $G(\mathbf{y}|\mathbf{x})$  and the VSP Green's functions  $G(\mathbf{A}|\mathbf{x})$  into the frequency domain.
- 4) Redatum the SSP data to the new datum using equation 1.
- 5) Transform the redatumed data into the time domain.

In the frequency domain, the algorithm can be implemented in parallel on a distributed cluster. The gain in computation efficiency with the target-oriented approach occurs because the number of band-limited Green's functions computed for sources on the new datum is significantly fewer than that on the original datum at the surface.

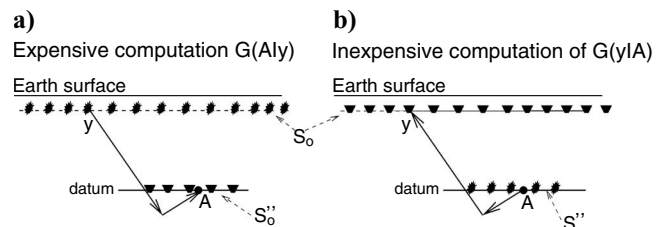


Figure 2. Computationally (a) expensive (with 13 FD solutions) and (b) inexpensive (with only five FD solutions) procedures for computing the extrapolation Green's function  $G(\mathbf{A}|\mathbf{y})$  in equation 1.

**Table 1.** Computation cost comparisons between standard and target-oriented RTD, where  $N_x^{src}$  and  $N_y^{src}$  are the numbers of sources in the  $x$ - and  $y$ -directions, respectively, and 195 FD denotes the fact that 195 shot gathers need to be calculated by a finite-difference method. In the 2D SEG/EAGE salt example, the length of the target's top boundary is the same as the top surface. Therefore, standard and target-oriented RTD in this case have the same computation costs. In the 3D examples, the target's top boundary is smaller than the top surface, and target-oriented RTD save up to 90% of computation costs.

	Surface area	Target area	Surface $N_x^{src}$	Surface $N_y^{src}$	Target $N_x^{src}$	Target $N_y^{src}$	Standard RTD cost	Target RTD cost
2D SEG/EAGE salt example	7.8 km	7.8 km	195	1	195	1	195 FD	195 FD
3D SEG/EAGE salt example	7.0 km <sup>2</sup>	3.3 km <sup>2</sup>	20	85	10	80	1700 FD	800 FD
3D GOM example	60.0 km <sup>2</sup>	6.0 km <sup>2</sup>	500	100	100	50	50,000 FD	5000 FD

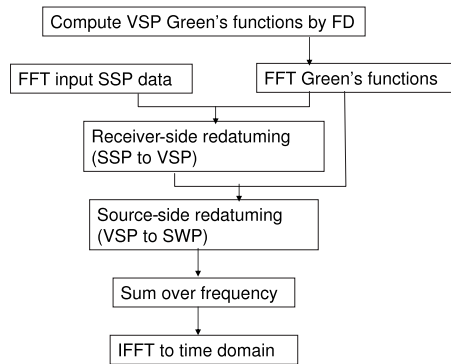


Figure 3. The workflow of target-oriented reverse-time datuming, which can be implemented in parallel on a cluster in the frequency domain.

Because a two-way wave equation is solved by the FD method, artificial reflections from velocity contrasts within the model are a significant source of noise. Two strategies are used to suppress the undesired reflections. First, a properly smoothed model is used to calculate the Green's functions, which can attenuate the backscattered waves without altering the wave propagation kinematics noticeably (Versteeg, 1993; Gray, 2000). Second, the density is adjusted so that the acoustic impedance is constant, which can avoid normal-incidence reflections from a velocity interface (Baysal et al., 1983; McMechan, 1983; Whitmore, 1983).

Adjustments along the data edges and model boundaries play another significant role in reducing artificial reflections from the edges. To reduce these artifacts, a cosine taper is applied over one wavelength along the edges of the original SSP survey. During the finite-difference computations, absorbing boundary conditions (Clayton and Engquist, 1977, 1980; Cerjan et al., 1985) are applied at the side and bottom boundaries. These steps attenuate most artificial reflections from model boundaries.

## NUMERICAL TEST

To demonstrate the effectiveness of the target-oriented RTD method, we implement this algorithm on 2D and 3D SEG/EAGE synthetic data and a 3D field data set from the Gulf of Mexico. For comparison, we migrate the redatumed data as well as the original seismic data recorded at the top surface using a Kirchhoff migration method.

### 2D synthetic data test

Synthetic examples associated with the 2D SEG/EAGE salt model in Figure 4 are used to test the target-oriented RTD method. A finite-difference solution to the 2D acoustic wave equation is used to compute the seismograms with a 15-Hz peak-frequency Ricker wavelet as the source wavelet. For the SSP geometry in the salt model, there are 195 shots and 195 receivers at 40-m intervals on the model surface. A typical common-shot gather (CSG) is shown in Figure 5a. To calculate the VSP Green's functions, 195 shots at 40-m intervals are placed along the horizontal datum line that is 0.5 km beneath the surface, and 195 receivers at 40-m intervals are located along the same surface. We refer to these traces as band-limited Green's functions because the source is not impulsive in time. Figure 5b shows a typical VSP band-limited Green's function.

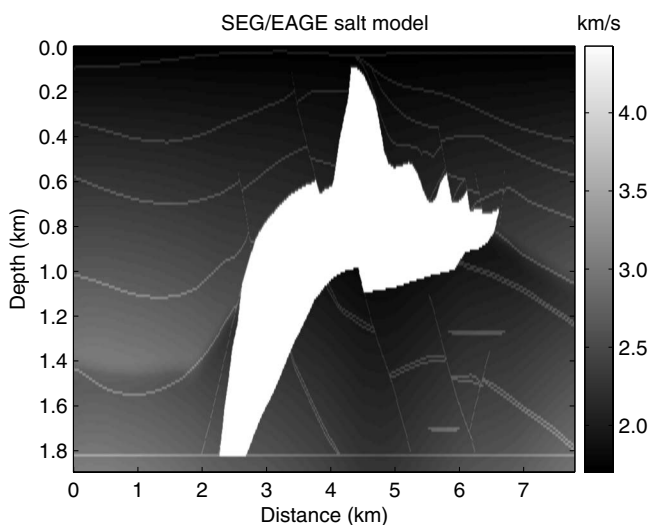


Figure 4. Two-dimensional SEG/EAGE synthetic salt model used for a 2D test, where the SSP experiment is synthesized with 195 shots and receivers, which are deployed evenly on the surface with a 40-m interval.

Equation 1 is used to redatum the SSP data so that the redatumed sources and receivers are distributed virtually along the new horizontal datum at a depth of 0.5 km. To check the accuracy of the redatumed data, we also computed a finite-difference solution to the 2D wave equation for a shot at the datum. Comparing this redatumed virtual CSG with the true CSG (Figure 6a and b) shows that the major events are accounted for correctly, but there are some artifacts in the redatumed traces. These blemishes result mostly from the far-field approximation and the finite aperture of the sources and receivers on the surface.

To test the effectiveness of the target-oriented RTD method for a subsalt target, we also redatumed the SSP data to a depth of 1.2 km, which is just below the salt dome in the model. Kirchhoff migration (KM) images are computed using the surface data and the redatumed data. The entire velocity model is used for Kirchhoff migration of SSP traces, although only the subsalt velocity model is needed to migrate the redatumed data. Figure 7 shows the zero-offset data of the original SSP and the redatumed gathers. The comparison shows that the redatumed traces have less complexity than those along the top surface and are less contaminated by diffraction energy associated with the salt bottom. The defocusing effects of the salt are avoided by redatuming below the salt.

Figure 8b and c show reflector images from Kirchhoff migration of the SSP data before and after datuming, respectively. For compar-

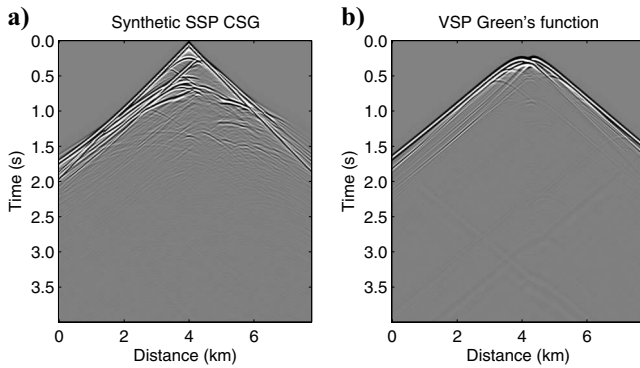


Figure 5. (a) Shows SSP synthetic seismograms generated by placing sources and receivers at the surface of the 2D SEG/EAGE model. (b) The VSP Green's function generated by placing sources at a depth of 0.5 km and receivers at the surface of the same model.

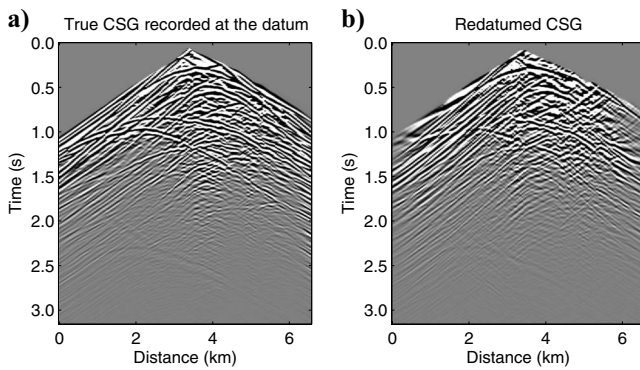


Figure 6. (a) True and (b) redatumed common-shot gather with sources and receivers at a depth of 0.5 km in the model depicted in Figure 4.

ison, the RTM image of the original SSP data is shown in Figure 8d. The subsalt portion of the images computed from the redatumed data is of higher quality than the KM image obtained from the original surface data. It is comparable to the RTM image. This is because the standard Kirchhoff migration of SSP data is single-arrival based, where the first arrivals below the salt are typically weak because of defocusing from the salt. In contrast, the redatumed data below the salt are obtained by transforming many of these defocused early arrivals to strongly focused arrivals. Computation time for this redatumed approach is less than one-third that of standard RTM.

### 3D synthetic data test

The 3D target-oriented RTD algorithm is tested on synthetic data associated with the 3D SEG/EAGE salt model. This model has a

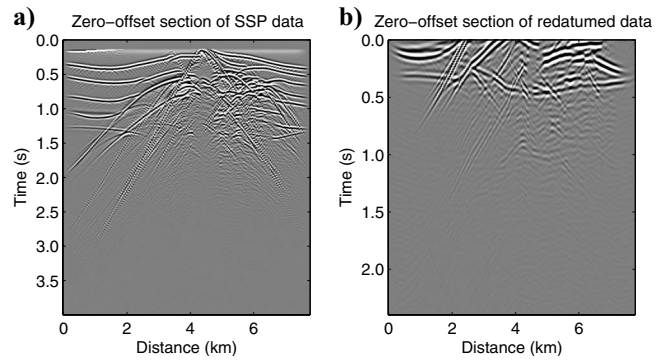


Figure 7. Zero-offset data (a) before and (b) after redatuming to a horizontal line at a depth of 1.2 km. Reflections in (b) are less complex and have fewer diffraction events compared to (a).

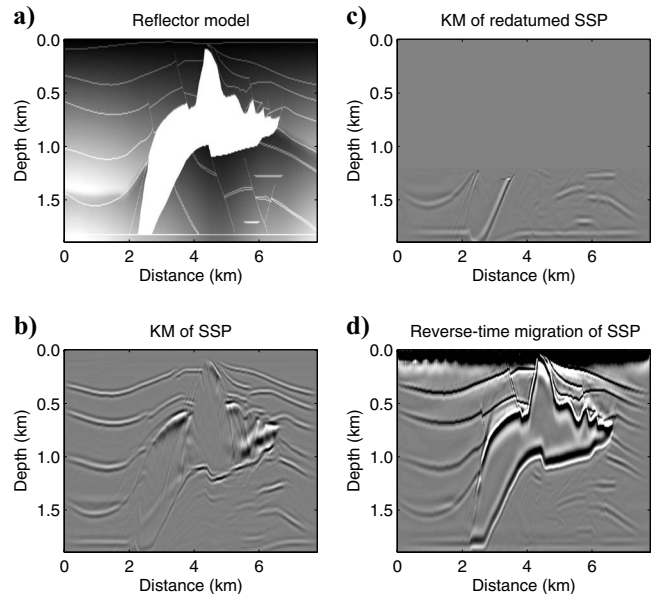


Figure 8. (a) Migration images below the datum depth of 1.2 km. Reflectivity images after (b) Kirchhoff migration of the SSP data, (c) Kirchhoff migration of redatumed SSP data. (d) Reverse-time migration of SSP data. Quality of the Kirchhoff migration image after redatuming is much clearer and has higher fidelity compared to the image before redatuming. The subsalt image is comparable to that of the reverse-time migration result with about 70% less calculation effort.

complicated structural nature, which is representative of salt intrusions in the Gulf of Mexico. Because of computer limitations, only part of the model is used to generate the synthetic data and test the target-oriented RTD algorithm. Figure 9 illustrates the velocity model 4.0 km along the  $x$ -direction and 2.0 km along the  $y$ -direction. A finite-difference solution to the 3D acoustic wave equation is used to compute the seismograms with a 15-Hz peak-frequency Ricker wavelet as the source wavelet. For the SSP geometry in the salt model, there are 1700 shots and receivers distributed evenly in 20 inlines and 85 crosslines. Source and receiver intervals are 40 m in the inline direction and 100 m in the crossline direction. Figure 10a shows a typical common-shot gather of synthetic SSP seismograms. To reveal structures below the salt dome, we redatum the SSP data to a datum at a depth of 1.2 km. Therefore, 800 VSP Green's functions are calculated by placing sources at the new datum and 1700 receivers at the near surface.

Equation 1 and a finite-difference method are used to redatum the SSP data to the new datum. Figure 10b shows a typical redatumed common-shot gather. Kirchhoff migration is applied to these redatumed data. For comparison, Kirchhoff migration is applied to the SSP data using the entire velocity model. Figures 11 and 12 are the corresponding 3D image cubes obtained by migrating the original data and redatumed data, respectively. The subsalt portion of the im-

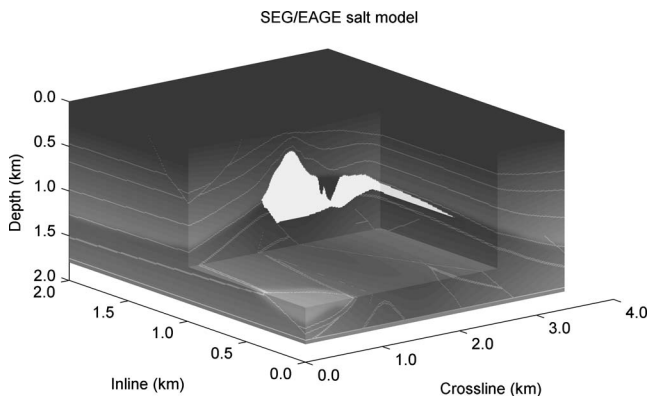


Figure 9. Three-dimensional SEG/EAGE synthetic salt model used for a 3D test, where the SSP experiment is synthesized with  $85 \times 22$  shots and receivers that are deployed evenly on the surface with a 40-m interval.

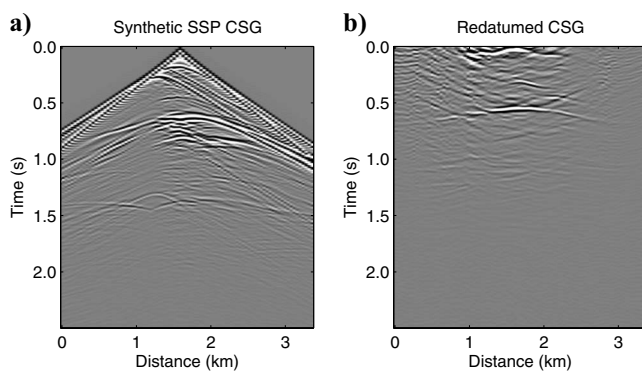


Figure 10. (a) A common-shot gather of SSP synthetic seismograms generated from model depicted in Figure 9. (b) Redatumed common-shot gather with sources and receivers at a depth of 1.5 km below the surface.

age in Figure 12 shows a higher quality than the corresponding KM image obtained from the surface data (Figure 11). To compare image quality in detail, different 2D slices of the image cubes are shown. Figure 13a and b show 3D Kirchhoff migration images of the SSP data before and after redatuming, respectively, at inline 41. The reflector model along this inline section is depicted in Figure 13c. Figure 14a and b depict the 3D Kirchhoff migration images of the SSP data before and after redatuming at crossline 161, respectively. Figure 15a and b show 3D Kirchhoff migration images of the SSP data before and after redatuming at the depth of 1.4 km, respectively. Comparisons at different inlines, crosslines, and depth slices show that subsalt migration images from the original SSP data are contaminated with noise and artifacts. In migration images from the redatumed data, we can identify reflectors at their correct locations. These comparisons indicate that target-oriented RTD can alleviate some of the defocusing effects of the salt significantly.

Computation times for this test are listed in Table 2. For comparison, the computation time of standard RTM is estimated based on the same data set and velocity model. Results show target-oriented RTD has a speedup factor of about ten over standard RTM, which can be attributed to two factors. First, a bottom-up approach is employed on a smaller datum area. Second, FD calculation of the Green's functions was restricted to the computation grid at and above the datum.

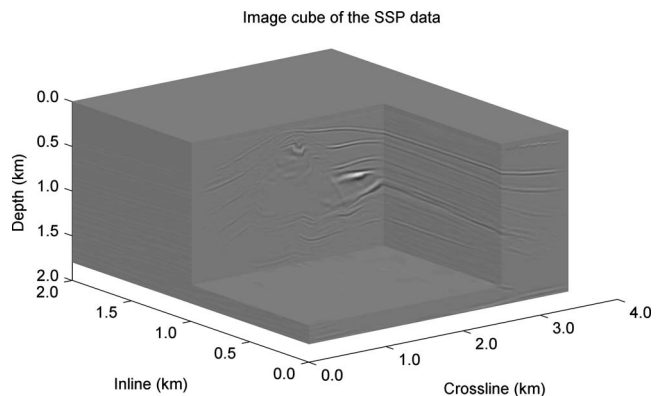


Figure 11. Stacked image after 3D Kirchhoff migration of SSP data.

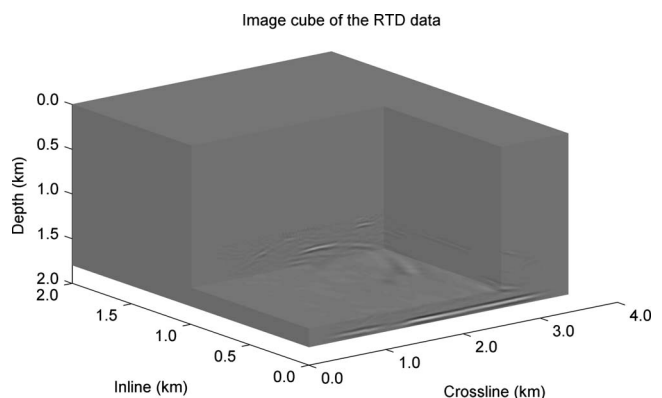


Figure 12. Stacked image after 3D Kirchhoff migration of the redatumed data.

3D field data test

We implement the target-oriented RTD method on a marine field data set recorded in Campeche Bay in the Gulf of Mexico (Figure 16). The seismic survey covers a rectangular area of 25 km by 20 km. In this area, the geological structures consist of an arcuate se-

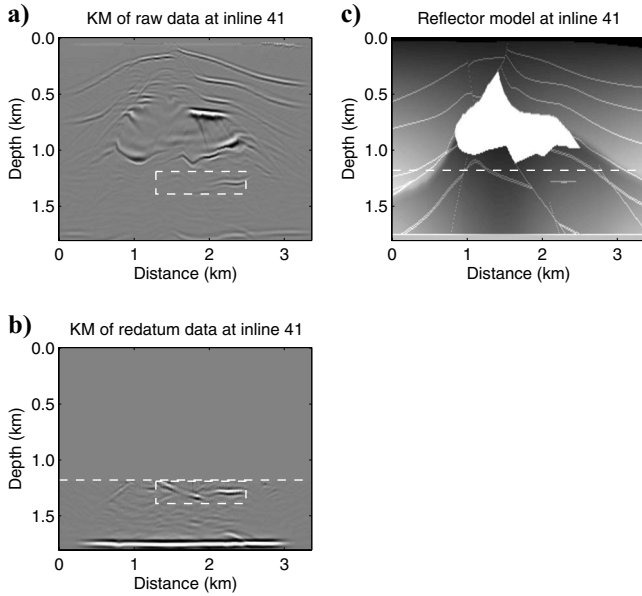


Figure 13. Two-dimensional slices of the 3D migration image cubes at inline 41: (a) Kirchhoff migration image of the original surface seismic gathers. (b) Kirchhoff migration image of redatumed data. (c) True reflector model. Horizontal dashed line indicates position of the new datum. Comparison between reflector images in boxed areas shows a noticeable improvement of image quality for the redatumed data.

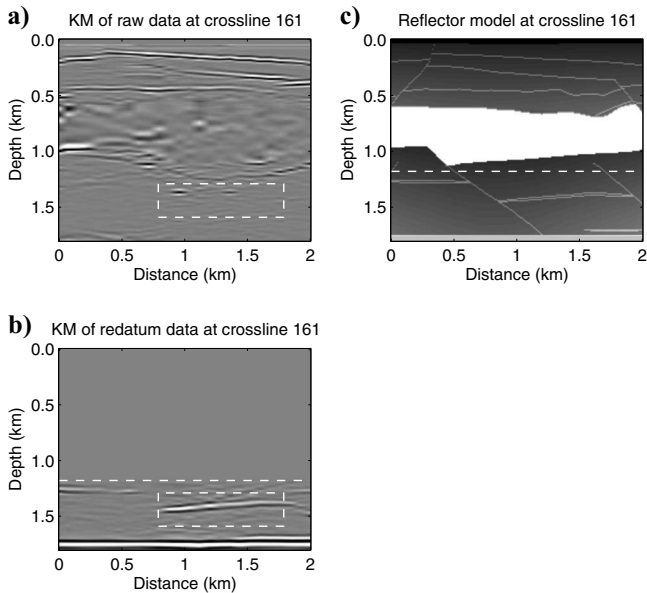


Figure 14. Two-dimensional slices of the 3D migration image cubes at crossline 161: (a) Kirchhoff migration image of the original surface seismic gathers. (b) Kirchhoff migration image of the redatumed data. (c) True reflector model.

ries of fold-thrust structures, which change orientation from approximately east-west to north-northwest-south-southeast (Mitra et al., 2006). The interval velocity model (Figure 17) shows large velocity gradients and high velocity variations in this area, which might cause serious defocusing effects in a seismic survey. Because of the complex wavefield, it is a challenge to reveal the structures in the deep area. Our goal is to redatum the surface seismic data to a deep datum close to the target zone and improve the image quality in this deep area.

The original seismic data were recorded by an ocean-bottom cable (OBC) system. Pressure seismograms are recorded by hydrophones on the sea floor (about 60 m below the sea level). More than 50,000 shots are distributed along 500 inlines and 100 crosslines. The shot intervals are 50 m in the inline direction and 200 m in the crossline direction, and the recorded time sampling interval is 4 ms. Figure 18a depicts a typical shot gather of the data. We redatumed the OBC data to a target area 1.5 km below sea level. A finite-difference solution to the 3D acoustic wave equation is used to compute the band-limited VSP Green’s function in Equation 1 with a 25-Hz peak-frequency Ricker wavelet as the source wavelet. More than 5000 shots

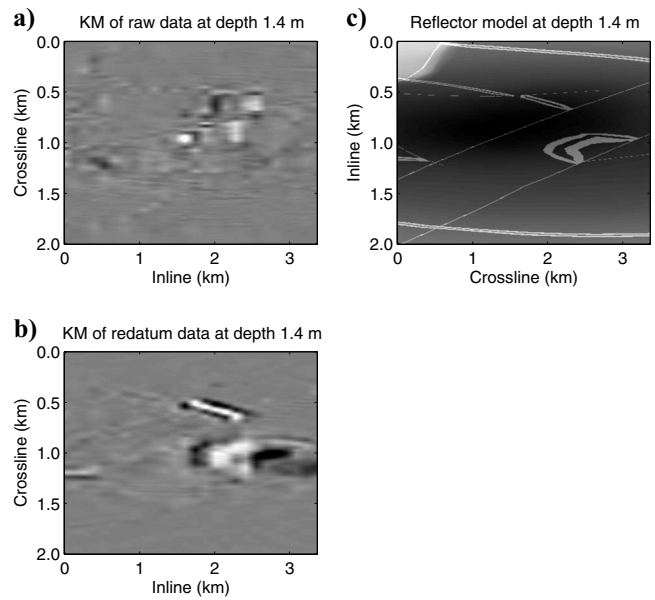


Figure 15. Two-dimensional slices of the 3D migration image cubes at a depth of 1.4 km: (a) Kirchhoff migration image of the original surface seismic gathers. (b) Kirchhoff migration image of the redatumed data. (c) True reflector model

Table 2. Computation CPU costs for different numerical tests, where calculations are based on a Linux cluster consisting of 64 2.0 GHz dual-core processor nodes.

Numerical tests	RTM (CPU-hours)	RTD (CPU hours)	Saving rate
2D SEG/EAGE synthetic test	21.0	6.5	69%
3D SEG/EAGE synthetic test	16,000 (est.)	1866	88%
3D field data test	5,000,000 (est.)	52,000	99%

are located along the new datum to calculate the band-limited VSP Green's functions compared to 50,000 shots in the original survey.

Equation 1 is used to redatum these OBC data to the new datum, Figure 18b shows a redatumed virtual shot gather. Kirchhoff migration is applied to the original OBC data and the redatumed data, where the entire velocity model is used for Kirchhoff migration of SSP traces although only the velocity below the datum is needed to migrate the redatumed data. Figures 19 and 20 show the corresponding 3D image cubes obtained by migrating the original data and redatumed data respectively. The deep portion of the image in Figure 20 is of higher quality than the KM image obtained from the surface data in Figure 19.

To compare image quality in detail, slices of the image cubes are shown. Figure 21a and b show 3D Kirchhoff migration images of the SSP data before and after redatuming, respectively, at inline 21. Another inline example is shown in Figure 22a and b. Figures 23 and 24 show the migration images at crosslines 61 and 101, and Figures 25

and 26 show the migration images at different depths of 2.0 km and 2.5 km. From these images, we can see more details of the deep reflectors. It is easier to identify faults and continuous reflectors from images of redatumed data than from the images of original data. Comparisons indicate that defocusing effects, multiples, and turning waves caused by the complex structures are relieved by the target-oriented RTD algorithm.

Computation time of the field data test is listed in Table 2. Compared to the estimated computation time for standard RTM, target-

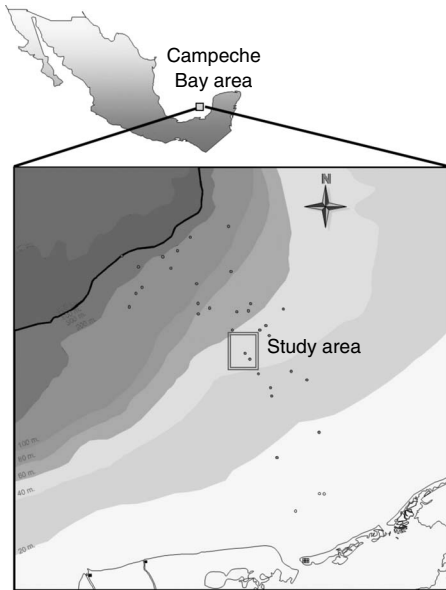


Figure 16. Study area for the 3D marine data from Campeche Bay area, Gulf of Mexico.

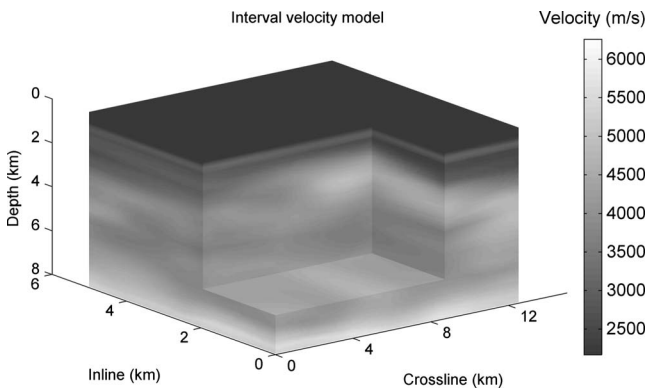


Figure 17. The 3D interval velocity model for the field data from the Gulf of Mexico. Original OBC data are redatumed to a new datum along a depth of 1.5 km below the surface. The VSP Green's functions are calculated by using the upper part of this model above the new datum.

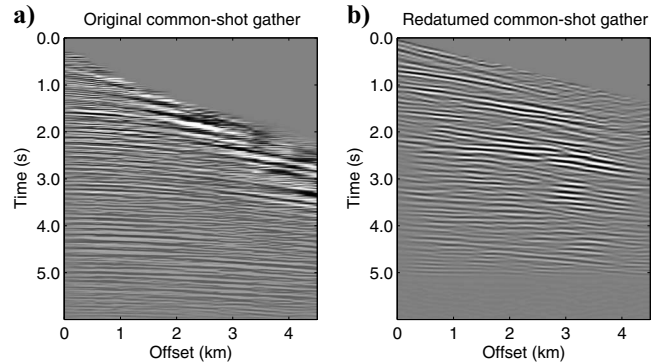


Figure 18. (a) A typical common-shot gather of the original OBC data, where the source is near sea surface and receivers are about 60 m below the sea surface. (b) A redatumed common-shot gather, where source and receivers are redatumed to the plane 1.5 km below the sea surface.

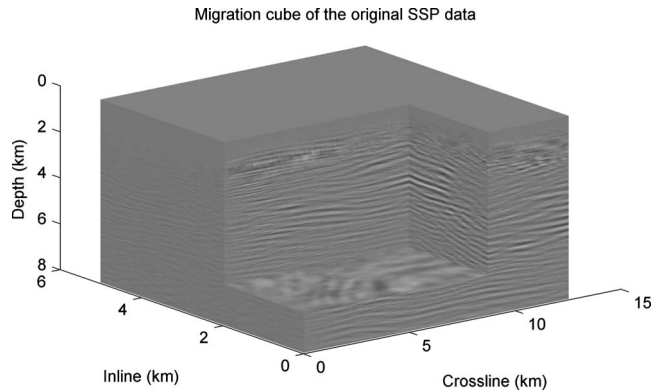


Figure 19. Stacked image after 3D Kirchhoff migration of SSP data.

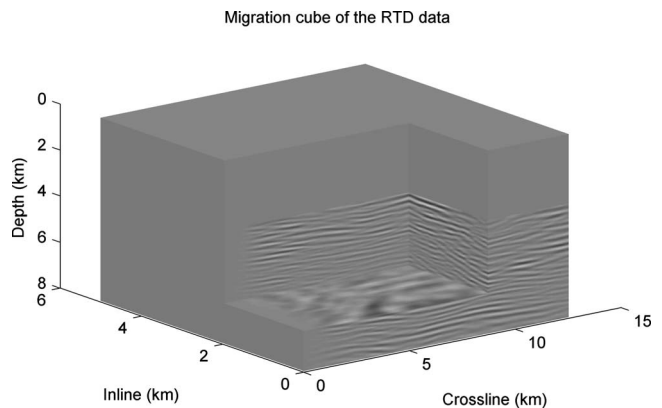


Figure 20. Stacked image after 3D Kirchhoff migration of redatumed data.

oriented RTD indicates a speedup factor of about one hundred over standard full-volume RTM. In this case, the efficiency is attributed to two factors. First, a bottom-up approach is applied to a small target area, which is only one-tenth of the surface survey area (see Table 1). Second, FD calculations were applied to the computation grid at and above the datum.

DISCUSSION

We applied RTD equations to the SSP traces associated with the 2D and 3D SEG/EAGE salt models. The redatumed data compared well with the actual shot gathers with sources and receivers located at the new datum, and the migrated redatumed data revealed the deep structures beneath the salt more clearly. This is because the redatumed data mostly have been corrected of the defocusing effects of the salt. In addition, we implemented target-oriented RTD on a field data set from the Gulf of Mexico. This field example demonstrates that this method works well with field data in the sense that it pro-

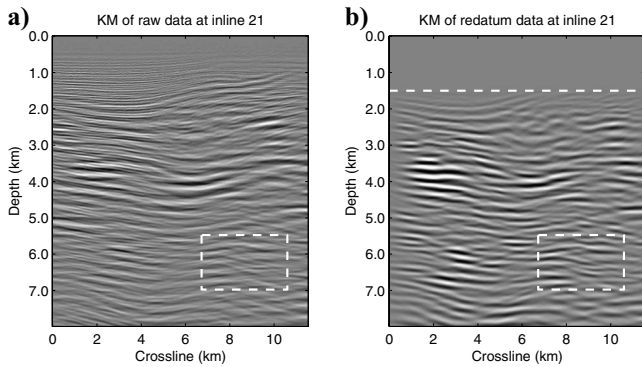


Figure 21. Two-dimensional slices of the 3D migration image cubes at inline 21: (a) Kirchhoff migration image of the original surface seismic gathers. (b) Kirchhoff migration image of the redatumed data.

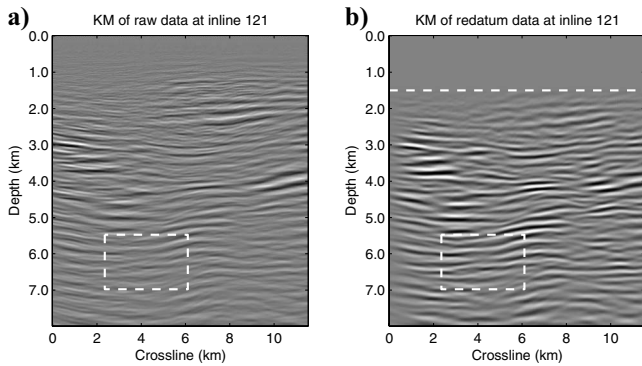


Figure 22. Similar to Figure 21 except that the 2D slices are at inline 121.

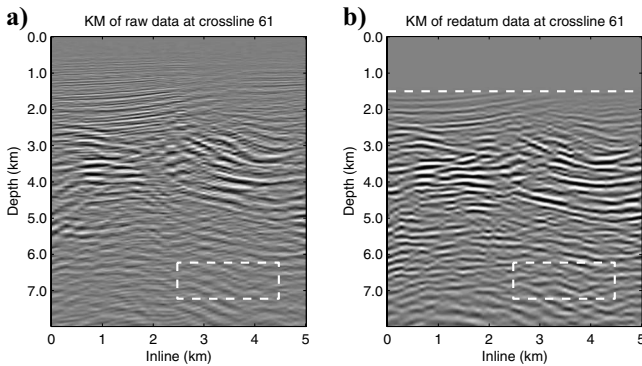


Figure 23. Two-dimensional slices of the 3D migration image cubes at crossline 61: (a) Kirchhoff migration image of the original surface seismic gathers. (b) Kirchhoff migration image of the redatumed data.

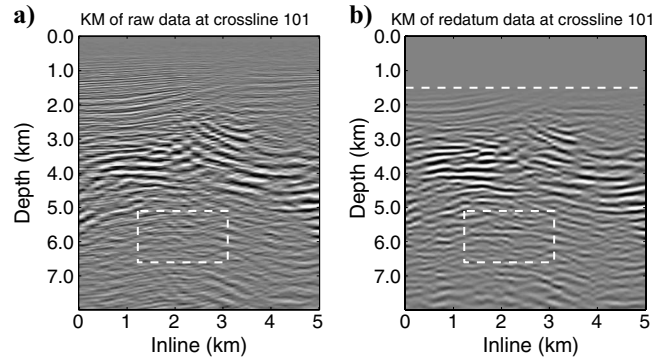


Figure 24. Similar to Figure 23 except that the 2D slices are at crossline 101.

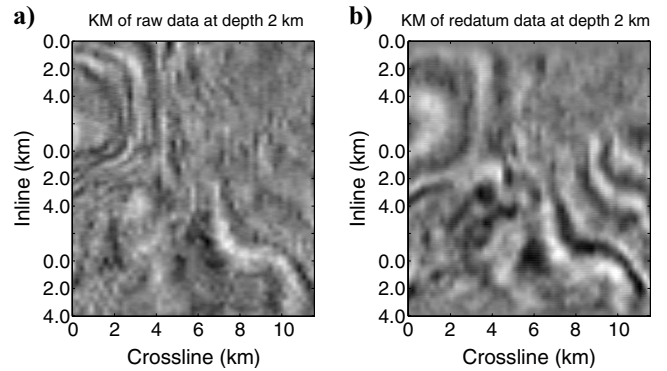


Figure 25. Two-dimensional slices of the 3D migration image cubes at a depth of 2.0 km: (a) Kirchhoff migration image of the original surface seismic gathers. (b) Kirchhoff migration image of the redatumed data.

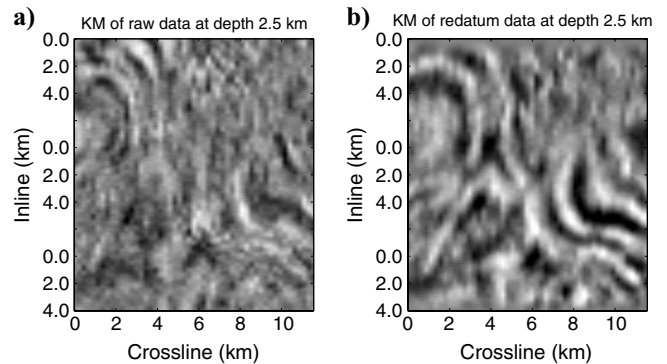


Figure 26. Similar to Figure 25 except that the 2D slices are at the depth of 2.5 km below the surface.

vides clear images of the subsurface reflectivity structure, despite the acoustic and Born approximations in this migration method. In contrast to the synthetic data example, these GOM data are associated with complex geology composed by carbonates and clastics but do not contain the strong lateral velocity contrasts of salt structures. Migration images from the redatumed data reveal deep reflectors and faults in the target areas better than migration images from the Kirchhoff original seismic data.

A merit of RTD is that, instead of using wavefield extrapolation at every grid point between the surface and the datum, it uses the cross-correlation of seismic data at the surface and the Green's functions with sources at the datum and receivers at the surface. The Green's functions are obtained by forward modeling, which means the computation efficiency of RTD also can be improved once a faster wave-equation modeling method is achieved. It also means that least-squares redatuming can be inexpensive because the Green's functions can be reused for modeling and redatuming at each iteration.

Using the bottom-up approach and target-oriented strategy, we can achieve much greater computation efficiency compared to standard RTD by wave extrapolation. This is because when we calculate the VSP Green's functions, the sources are placed at the new datum, which typically has a smaller area than that covered by the sources along the top surface. Computation costs for all numerical tests are summarized in Table 2, where the calculations are based on a Linux cluster consisting of 64 2.0 GHz dual-core processor nodes.

RTM is approaching shot-profile migration (SPM) speed through orders-of-magnitude faster wave-equation modeling. However, as technology improves, computation cost and disk space usage become less critical. This reduces the practical application of RTD, but the method still has some advantages over traditional imaging approaches. First, RTD can speed up by using the same wave-equation modeling technology. Second, RTD yields target-oriented data sets,

and any imaging methods and velocity-analysis technologies can be used on these data sets to achieve a target-oriented application. For example, salt-model building usually needs migration several times in the same area. In this case, full-volume migration is available but not necessary. A potential application of RTD is the target-oriented velocity analysis. The redatumed data can be used for velocity-model building for the target area below the overburden. The redatumed data have a shorter recording time and a narrower offset range compared to the original SSP data. Most importantly, the redatumed data generally have simpler seismic events because the distorting effects and the refraction waves caused by the overburden are avoided by the redatuming process. Thus, the speed and the quality of velocity-model building can be improved using redatumed data.

## CONCLUSIONS

We present a reverse-time-datuming method, which can generate redatumed data economically in target areas. Computation savings are achieved through limiting Green's functions related to target areas by using a bottom-up strategy. This method can handle complex structures and strong lateral velocity variations of the overburden properly when surface sources and receivers are redatumed to be below it. This can be important for subsalt imaging. Better resolution of the target can be achieved because redatumed sources and receivers are closer to the target, and multiple arrivals that propagate from the surface to the datum are used for imaging below the overburden. Several example migration images from the redatumed data reveal the deep reflectors and faults in the target areas better than images from standard Kirchhoff migration. Although the datum area is required to be much smaller than the original surface acquisition area, bottom-up RTD is still a promising method for target-oriented imaging and velocity updating. Storage requirements of the band-limited Green's functions are a challenge. Storage requirements are related proportionally to the area of the target zone. Thus, target-oriented RTD works well mainly in the case where the target zone is much smaller than the seismic survey area.

## ACKNOWLEDGMENTS

We thank the sponsors of the University of Utah Tomography and Model/Migration (UTAM) Consortium for their support. We thank PEMEX Exploration and Production for permission to use and publish the data.

## APPENDIX A

### SSP → SWP TRANSFORM

Redatuming of surface seismic data to a deeper horizontal datum is equivalent to the SSP → SWP correlation transform obtained by a concatenation of the SSP → VSP and VSP → SWP transforms. These operations are described by the acoustic reciprocity equation of correlation type (Wapenaar, 2004; Schuster, 2009) and presented in the next sections.

### SSP → VSP TRANSFORM

The starting point for the derivation of the SSP → VSP transform is the model depicted in Figure 27a where  $x$  and  $y$  are the locations of sources and receivers near the surface, and  $A$  and  $B$  are along the da-

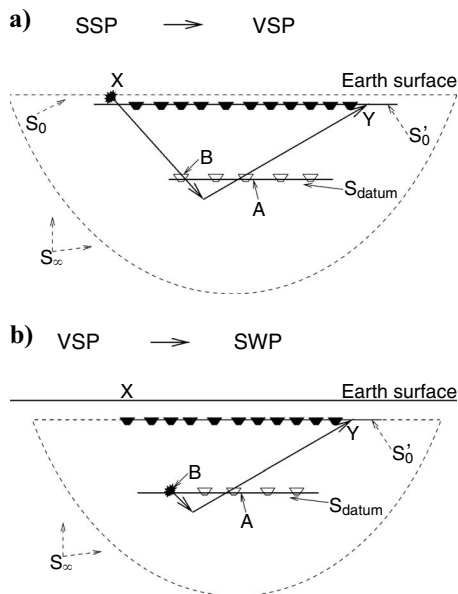


Figure 27. Diagram demonstration for (a) VSP → SWP correlation transform. Integration surface denoted by dashed line. The VSP receivers are along  $S_0$  and the sources are distributed along the datum line  $S_{datum}$ . Open geophones indicate the locations of virtual geophones at the datum. (b) VSP → SWP correlation transform. The VSP receivers are along  $S'_0$  and sources are distributed along the datum line  $S_{datum}$ .

tum line. This configuration of sources and receivers is employed for a simultaneous VSP and SSP experiment. Using the dashed contour (and its infinite extension out of the page) defines the surface of 2D integration to give the SSP → VSP correlation transform:

$$\begin{aligned} & \mathbf{B} \in S_{datum}, \mathbf{y} \in S'_0; \quad 2i \overbrace{Im[G(\mathbf{A}|\mathbf{y})]}^{VSP} \\ &= \int_{S_0 + S_z} \left[ G(\mathbf{B}|\mathbf{x})^* \frac{\partial G(\mathbf{y}|\mathbf{x})}{\partial n_x} - G(\mathbf{y}|\mathbf{x}) \frac{\partial G(\mathbf{B}|\mathbf{x})^*}{\partial n_x} \right] d^2x, \\ &\approx \int_{S_0} \left[ \overbrace{G(\mathbf{B}|\mathbf{x})^*}^{VSP} \frac{\partial \overbrace{G(\mathbf{y}|\mathbf{x})}^{SSP}}{\partial n_x} - \overbrace{G(\mathbf{y}|\mathbf{x})}^{SSP} \frac{\partial \overbrace{G(\mathbf{B}|\mathbf{x})^*}^{VSP}}{\partial n_x} \right] d^2x, \end{aligned} \quad (\text{A-1})$$

where  $G(\mathbf{B}|\mathbf{x})$  is the Green's function for a harmonic point source in an acoustic medium with variable velocity and constant density, and  $n_x$  is along the normal direction to the integration surface. The integration over the half circle at infinity can be neglected by the Wapenaar anti-radiation condition (Wapenaar, 2006). Here,  $S_0$  is the surface along which the airgun sources are excited; and  $G(\mathbf{B}|\mathbf{x})$  for the integration along  $\mathbf{x} \in S_0$  denotes the VSP Green's function where the receiver at  $\mathbf{B}$  is along the datum line, which can be considered as a buried well. In contrast,  $G(\mathbf{y}|\mathbf{x})$  is the SSP Green's function where both the source and receiver are near the surface.

The far-field approximation to the above equation yields (Wapenaar, 2004; Schuster, 2009)

$$\begin{aligned} & \mathbf{B} \in S_{datum}, \mathbf{y} \in S'_0; \quad \overbrace{G(\mathbf{y}|\mathbf{B}) - G(\mathbf{y}|\mathbf{B})^*}^{VSP} \\ &= 2ik \int_{S_0} \overbrace{G(\mathbf{B}|\mathbf{x})^*}^{VSP} \overbrace{G(\mathbf{y}|\mathbf{x})}^{SSP} d^2x, \end{aligned} \quad (\text{A-2})$$

which is the SSP → VSP correlation transform which redatums the SSP shots near the sea surface to the new datum.

### VSP → SWP CORRELATION TRANSFORM

Similar to the previous transform, the receivers near the sea surface can be redatumed to the new datum line. Figure 27b demonstrates the model used for this transform, where  $\mathbf{y}$  are the locations of the VSP receivers near the surface and  $\mathbf{B}$  is the VSP source located at the datum line. The dashed contour defines the surface of 2D integration to give the VSP → SWP correlation transform. Based on the Wapenaar anti-radiation condition and far-field approximation, the VSP → SWP transform can be described by:

$$\mathbf{A}, \mathbf{B} \in S_{datum}; \quad \overbrace{Im[G(\mathbf{A}|\mathbf{B})]}^{SWP} = k \int_{S'_0} \overbrace{G(\mathbf{A}|\mathbf{y})^*}^{VSP} \overbrace{G(\mathbf{B}|\mathbf{y})}^{VSP} d^2y. \quad (\text{A-3})$$

Using the reciprocity principle in equation A-2, we get an expression

for  $G(\mathbf{B}|\mathbf{y})$ :

$$\begin{aligned} \mathbf{B} \in S_{datum}, \mathbf{y} \in S'_0; \quad \overbrace{G(\mathbf{B}|\mathbf{y})}^{VSP} &= 2ik \int_{S_0} \overbrace{G(\mathbf{B}|\mathbf{x})^*}^{VSP} \overbrace{G(\mathbf{y}|\mathbf{x})}^{SSP} d^2x \\ &+ G(\mathbf{B}|\mathbf{y})^*. \end{aligned} \quad (\text{A-4})$$

Inserting  $G(\mathbf{B}|\mathbf{y})$  from the above equation into equation A-3 yields the SSP → SWP transform

$$\begin{aligned} \mathbf{A}, \mathbf{B} \in S_{datum}; \quad \overbrace{Im[G(\mathbf{A}|\mathbf{B})]}^{SWP} \\ &= 2ik^2 \int_{S_0} \int_{S'_0} \overbrace{G(\mathbf{A}|\mathbf{y})^*}^{VSP} \overbrace{G(\mathbf{y}|\mathbf{x})}^{SSP} \overbrace{G(\mathbf{B}|\mathbf{x})^*}^{VSP} d^2y d^2x \\ &+ \int_{S'_0} G(\mathbf{A}|\mathbf{y})^* G(\mathbf{B}|\mathbf{y})^* d^2y, \end{aligned} \quad (\text{A-5})$$

where reciprocity is invoked to interchange source and receiver locations in the SSP data  $G(\mathbf{x}|\mathbf{y})$ . The last integral on the right-hand side has a kernel that is a product of acausal Green's functions, which will not contribute to the redatumed traces after  $t \geq 0$ . Therefore, this last integral is ignored if the redatumed data are migrated to deeper depths so that we have

$$\begin{aligned} \mathbf{A}, \mathbf{B} \in S_{datum}; \quad \overbrace{Im[G(\mathbf{A}|\mathbf{B})]}^{SWP} \\ \approx 2ik^2 \int_{S_0} \int_{S'_0} \overbrace{G(\mathbf{A}|\mathbf{y})^*}^{VSP} \overbrace{G(\mathbf{y}|\mathbf{x})}^{SSP} \overbrace{G(\mathbf{B}|\mathbf{x})^*}^{VSP} d^2y d^2x. \end{aligned} \quad (\text{A-6})$$

Above is the equation for RTD. It is similar to the classical redatuming equation used in seismic exploration (Berryhill, 1979, 1984, 1986; Yilmaz and Lucas, 1986; Bevc, 1995) Equation 1 says that the RTD data can be obtained by two back-projections of the SSP data, one for the receiver positions and one for the source locations of  $G(\mathbf{y}|\mathbf{x})$ . The VSP Green's functions  $G(\mathbf{A}|\mathbf{y})$  and  $G(\mathbf{B}|\mathbf{x})$  can be computed using an assumed velocity model that is accurate.

### REFERENCES

- Baysal, D. E., D. Kosloff, and J. W. C. Sherwood, 1983, Reverse-time migration: *Geophysics*, **48**, 1514–1524.
- Berryhill, J. R., 1979, Wave-equation datuming: *Geophysics*, **44**, 1329–1344.
- , 1984, Wave-equation datuming before stack: *Geophysics*, **49**, 2064–2066.
- , 1986, Submarine canyons Velocity replacement by wave-equation datuming before stack: *Geophysics*, **51**, 1572–1579.
- Bevc, D., 1995, Imaging under rugged topography and complex velocity structure: Ph.D. thesis, Stanford University.
- Biondi, B., R. R. Glapp, M. Prucha, and P. Sava, 2002, 3D prestack wave-equation imaging: A rapidly evolving technology: EAGE workshop.
- Cao, W., 2007, Wave-equation wavefront migration: 77th Annual International Meeting, SEG, Expanded Abstracts, 2155–2159.
- Cerjan, C., D. Kosloff, and M. Reshef, 1985, A nonreflecting boundary condition for discrete acoustic and elastic wave equation: *Geophysics*, **50**, 705–708.
- Claerbout, J. F., 1971, Toward a unified theory of reflector mapping: *Geophysics*, **36**, 467–481.
- , 1985, *Imaging the earth's interior*: Blackwell Science, Inc.

- Clayton, W. R., and B. Engquist, 1977, Absorbing boundary conditions for acoustic and elastic wave equations: *Bulletin of the Seismological Society of America*, **67**, 1529–1540.
- , 1980, Absorbing boundary conditions for wave-equation migration: *Geophysics*, **45**, 1538–1551.
- Dong, S., X. Xiao, and G. T. Schuster, 2007, 3D target-oriented reverse-time datuming: 77th Annual International Meeting, SEG, Expanded Abstracts, 2442–2445.
- Esmersoy, C., and M. Oristaglio, 1988, Reverse-time wave-field extrapolation, imaging, and inversion: *Geophysics*, **53**, 920–931.
- Gray, S. H., 2000, Velocity smoothing for depth migration: How much is too much?: 70th Annual International Meeting, SEG, Expanded Abstracts, 1055–1058.
- Gray, S. H., J. Etgen, J. Dellinger, and D. Whitmore, 2001, Seismic migration problems and solutions: *Geophysics*, **66**, 1622–1640.
- Liu, W., and Y. Wang, 2008, Target-oriented reverse-time migration for two-way prestack depth imaging: 78th Annual International Meeting, SEG, Expanded Abstracts, 2326–2331.
- Luo, Y., and G. T. Schuster, 2004, Bottom-up target-oriented reverse-time datuming: CPS/SEG Geophysics Conference and Exhibition, F55.
- McMechan, G. A., 1983, Migration by extrapolation of time-dependent boundary values: *Geophysical Prospecting*, **31**, 413–420.
- Mitra, S., J. A. D. Gonzalez, J. G. Hernandez, S. H. Garcia, and S. Banerjee, 2006, Structural geometry and evolution of the Ku, Zaap, and Maloob structures, Campeche Bay, Mexico: *AAPG Bulletin*, **90**, 1565–1584.
- Schuster, G. T., 2002, Reverse-time migration = generalized diffraction stack migration: 72nd Annual International Meeting, SEG, Expanded Abstracts, 1280–1283.
- , 2009, *Seismic interferometry*: Cambridge University Press.
- Symes, W. W., 2007, Reverse-time migration with optimal checkpointing: *Geophysics*, **72**, no. 5, SM213–SM221.
- Versteeg, R. J., 1993, Sensitivity of prestack depth migration to the velocity model: *Geophysics*, **58**, 873–882.
- Wang, B., F. Audebert, D. Wheaton, and V. Dirks, 2006, Subsalt velocity analysis by combining wave equation based redatuming and Kirchhoff based migration velocity analysis: 76th Annual International Meeting, SEG, Expanded Abstracts, 2442–2445.
- Wapenaar, K., 2004, Retrieving the elastodynamic Green's function of an arbitrary inhomogeneous medium by cross correlation: *Physical Review Letters*, **93**, 254301-1–254301-4.
- , 2006, Green's function retrieval by cross-correlation in case of one-sided illumination: *Geophysical Research Letters*, **33**, L19304 doi: 10.1029/2006GL027747.
- Whitmore, N. D., 1983, Iterative depth migration by backward time propagation: 53rd Annual International Meeting, SEG, Expanded Abstracts, 382–385.
- Yilmaz, O., and D. Lucas, 1986, Prestack layer replacement: *Geophysics*, **51**, 1355–1369.
- Zhou, M., and G. T. Schuster, 2002, Wave-equation wavefront migration: 72nd Annual International Meeting, SEG, Expanded Abstracts, 1292–1295.